

## Spin-glass overlap barriers in three and four dimensions

Bernd A. Berg\*

*Department of Physics, The Florida State University, Tallahassee, Florida 32306  
and Supercomputer Computations Research Institute, The Florida State University, Tallahassee, Florida 32306*

Alain Billoire†

*CEA/Saclay, Service de Physique Théorique, 91191 Gif-sur-Yvette, France*

Wolfhard Janke‡

*Institut für Theoretische Physik, Universität Leipzig, D-04109 Leipzig, Germany*

(Received 1 October 1999; revised manuscript received 13 January 2000)

For the Edwards-Anderson Ising spin-glass model in three and four dimensions ( $3d$  and  $4d$ ) we have performed high statistics Monte Carlo calculations of those free-energy barriers  $F_b^q$  which are visible in the probability density  $P_{\mathcal{J}}(q)$  of the Parisi overlap parameter  $q$ . The calculations rely on the recently introduced multioverlap algorithm. In both dimensions, within the limits of lattice sizes investigated, these barriers are found to be non-self-averaging and the same is true for the autocorrelation times of our algorithm. Further, we present evidence that barriers hidden in  $q$  dominate the canonical autocorrelation times.

### I. INTRODUCTION

Spin glasses (for reviews, see Refs. 1–4) constitute an important class of materials whose low-temperature state is a frozen disordered one. In order to produce such a state, there must be randomness and frustration among the different interactions between the spins (magnetic moments). Frustration means that no single spin configuration is favored by all interactions. In real materials such competing interactions are, for instance, created by magnetic impurity moments. The study of spin glasses developed essentially since the middle of the 1970s and is based on three approaches: experiment, theory, and computer simulation.

Experimentally it is not hard to find spin glasses.<sup>2</sup> One kind of widely studied system consists of dilute solutions of transition-metal magnetic impurities in noble hosts. The impurity moments produce a magnetic polarization of the host metal conduction electrons which is positive at some distances and negative at others. Because of the random placements of the impurities they have random, competing interactions with one another. Spin-glass states have also been found in magnetic insulators and amorphous alloys. Properties analogous to those of spin glasses, with the electric dipole moment playing the role of the magnetic one, have been seen in ferroelectric-antiferroelectric mixtures. The universal behavior of the observed phenomena is a major reason for the interest in these systems.

A freezing temperature  $T_c$  may be defined by a cusp in the ac susceptibility and has, for instance, been studied for Cu-0.9% Mn.<sup>5</sup> Below this transition temperature characteristic nonequilibrium phenomena are observed. A typical experiment is the measurement of the remanent magnetization, see Ref. 6 for a study of  $(\text{Fe}_{0.15}\text{Ni}_{0.85})_{75}\text{P}_{16}\text{B}_6\text{Al}_3$ . A spin-glass sample is rapidly cooled in a magnetic field to a temperature below the transition temperature and the observation is that the decay of the magnetization depends on the waiting time after which the field is switched off. This phenomenon

is called aging and has also been found in other disordered or amorphous systems such as structural glasses, polymers, high-temperature superconductors, and charge-density wave systems. These large characteristic time scales suggest the presence of many equilibrium or metastable configurations with a distribution of free-energy barriers separating them.

For free-energy barriers in spin glasses a major complication arises from the fact that there is no parametrization of the relevant configurations by a conventional thermodynamic variable. In his work<sup>7</sup> on the mean-field theory of spin glasses Parisi generalized the concept of an order parameter. In later language<sup>1–4</sup> this is expressed as follows: A spin-glass realization is defined by a set of frozen, disordered exchange coupling constants  $\mathcal{J} = \{J_{ik}\}$  and for each realization the Parisi overlap parameter is defined by

$$q = \frac{1}{N} \sum_{i=1}^N s_i^1 s_i^2, \quad (1)$$

where the sum goes over the total number  $N$  of spins of the system and the spin superscripts label two (real) replica of the same realization. For given  $\mathcal{J}$  the probability density of  $q$  is denoted by  $P_{\mathcal{J}}(q)$  and its cumulative distribution function is  $x_{\mathcal{J}}(q) = \int_{-q}^q dq' P_{\mathcal{J}}(q')$ . Average over the disorder defines the functions

$$P(q) = [P_{\mathcal{J}}(q)]_{\text{av}} = \frac{1}{\#J} \sum_{\mathcal{J}} P_{\mathcal{J}}(q) \quad \text{and}$$

$$x(q) = [x_{\mathcal{J}}(q)]_{\text{av}} = \frac{1}{\#J} \sum_{\mathcal{J}} x_{\mathcal{J}}(q),$$

where  $\#J$  is the number of realizations considered. In the infinite volume limit below the freezing temperature an increasing *continuous* part of  $x(q)$  characterizes mean-field behavior of spin glasses, whereas in ferromagnets as well as in the droplet picture<sup>8</sup> of spin glasses  $x(q)$  is a step function.

Analytical calculations in mean-field theory show that violations of the fluctuation-dissipation theorem in nonequilibrium dynamics determine the static function  $x(q)$  and vice versa,<sup>9</sup> see Ref. 10 for a review. Numerical calculations in  $3d$  and  $4d$  Ising spin glasses<sup>11,12</sup> support that this relationship holds also in finite dimensions. Of course, the entire  $P_{\mathcal{J}}(q)$  set contains more information than its mean  $P(q)$  [equivalently  $x(q)$ ]. In this paper we study the distribution of the minima in  $q$  of the  $P_{\mathcal{J}}(q)$  probability densities. For given  $\mathcal{J}$  the nontrivial (i.e., away from  $q = \pm 1$ ) minima are related to free-energy barriers of the disordered system  $\mathcal{J}$ . The other way around, it is presumably model dependent (and worthwhile to investigate) to what extent free-energy barriers of the system  $\mathcal{J}$  are reflected in the minima of the  $P_{\mathcal{J}}(q)$  probability density.

Conventional, canonical Monte Carlo (MC) simulations do not allow for an efficient investigation of the  $P_{\mathcal{J}}(q)$  minima, because the likelihood to generate corresponding configurations in the Gibbs canonical ensemble is small. This problem is overcome by the multioverlap MC algorithm<sup>13</sup> which samples with a uniform distribution in  $q$ . It belongs to the class of multicanonical and related algorithms<sup>14,15</sup>, which allows us to focus on rare configurations of the Gibbs ensemble. For instance, at first-order phase transitions in  $3d$ , configurations with interfaces are suppressed according to  $\exp(-\sigma A_{\min})$ , where  $\sigma$  is the interface tension and  $A_{\min}$  is the minimal area of the interface. For temperature driven transitions configurations with interfaces are found for  $E$  in the energy range  $E_1 < E < E_2$  where  $E_2 = E_1 + \Delta E$  and  $\Delta E$  is the latent heat of the transition. To generate such configurations with a good statistics it is sufficient to sample with a weight factor  $w(E) \sim 1/n(E)$ , where  $n(E)$  is the spectral density. Similarly, interfaces for magnetic field driven first-order phase transitions can be generated by sampling with an appropriate weight function  $w(M)$  of the magnetization  $M$  of the sample.

Once  $P_{\mathcal{J}}(q)$  is determined, we define the associated free-energy barrier  $F_B^q$  through the autocorrelation time of a  $1d$  Markov process which has the canonical  $P_{\mathcal{J}}(q)$  distribution as equilibrium state. The barrier autocorrelation time  $\tau_B^q$  is then defined through the second largest eigenvalue of the transition matrix of this Markov process and the free-energy barrier is  $\ln(\tau_B^q)$ .

In previous literature,<sup>16–21</sup> investigations of spin-glass barriers relied on various numerical and analytical methods, which are distinct from ours. The results of Refs. 16–20 may be summarized as support of a scaling law  $F_B^{\text{can}} \sim N^{1/3}$  for canonical free-energy barriers in the mean-field limit below the freezing temperature.

In the next section we describe our methods and give an overview of our MC statistics. Section III presents and interprets our numerical results for free-energy barriers in  $q$ . Conclusions and an outlook are given in the final Sec. IV.

## II. OVERVIEW OF METHODS AND DATA

The energy of the Edwards-Anderson Ising (EAI) (Ref. 22) spin-glass model is given by

$$E = - \sum_{\langle ik \rangle} J_{ik} s_i s_k, \quad (2)$$

TABLE I. Statistics: Number of realizations  $\#\mathcal{J}$ , average number of megasweeps per realization  $n_{\text{sw}}$  and average single 375 MHz processor CPU time per realization in hours (h) or seconds (s) as benchmarked on the CEA T3E.

$L$	$3d$			$4d$		
	$\#\mathcal{J}$	$n_{\text{sw}}$	CPU	$\#\mathcal{J}$	$n_{\text{sw}}$	CPU
4	8 192	0.2 M	6.32 s	4 096	0.4 M	76.6 s
6	8 192	1.0 M	113 s	4 096	3.7 M	1.02 h
8	8 192	7.6 M	0.54 h	1 024	49.3 M	42.66 h
12	640	154.0 M	36.97 h			

where the sum is over nearest-neighbor pairs of a (hyper) cubic lattice. The spins  $s_i$  as well as the coupling constants  $J_{ik}$  take on the values  $\pm 1$ , with equal probabilities, i.e., the sum  $N^{-1} \sum_{\langle ik \rangle} J_{ik}$  is of order  $1/\sqrt{N}$ .

In our calculations we combine the two copies (replica) of the same realization and simulate with a weight function

$$w(q) = \exp[-\beta(E^1 + E^2) + S(q)]. \quad (3)$$

Here  $\beta = J_0/k_B T$  is the inverse temperature in natural units,  $E^1$  and  $E^2$  are the energies of the respective replicas, and  $S(q)$  has the meaning of the microcanonical entropy of the Parisi order parameter (1). The multioverlap algorithm weights spin configurations with an overlap parameter  $q$  in such a way that a broad histogram in  $q$ , eventually covering the entire accessible range  $-1 \leq q \leq 1$ , is obtained. This allows then for accurate calculations of the empirical probability density  $P_{\mathcal{J}}(q)$  of the Parisi order parameter for realization  $\mathcal{J}$ . Although an explicit order parameter does not exist, our simulation method<sup>13</sup> is in this way similar to the multimagnetical,<sup>15</sup> which for ferromagnetic systems is a very efficient way to sample configurations with interfaces.

Our EAI simulations are performed on  $N = L^d$  ( $d = 3, 4$ ) lattices at  $\beta = 1$  ( $3d$ ) and  $\beta = 0.6$  ( $4d$ ). Both values correspond to temperatures  $T = 1/\beta$  below the freezing temperature of the respective model [ $\beta_c = 0.90 \pm 0.03$  ( $3d$ ) (Ref. 23),  $\beta_c = 0.485 \pm 0.005$  ( $4d$ ) (Ref. 24)]. Table I summarizes the statistics we have assembled as well as the performance of our code. MC updates are given in units of *sweeps*. Our  $J_{ik}$

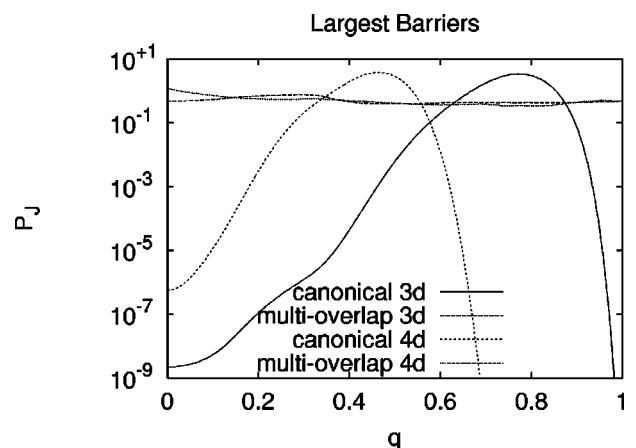


FIG. 1. Canonical  $P_{\mathcal{J}}(q)$  and (flat) multioverlap  $P_{\mathcal{J}}^{\text{muo}}(q)$  probability densities for our realization with the largest free-energy barrier in  $3d$  ( $L = 8$ ) and  $4d$  ( $L = 8$ ).

TABLE II. Mean, median, and maximum values for the Markov autocorrelations times  $\tau_B^q$  (8).

$L$	4	6	8	12
3d: mean	$61(29) \times 10^4$	$10(06) \times 10^6$	$56(45) \times 10^6$	$13(10) \times 10^7$
3d: median	$237(05) \times 10^1$	$690(02) \times 10^1$	$152(04) \times 10^2$	$444(05) \times 10^2$
3d: maximum	$22(20) \times 10^8$	$32(06) \times 10^9$	$35(33) \times 10^{10}$	$53(30) \times 10^9$
4d: mean	$94(34) \times 10^3$	$23(08) \times 10^5$	$26(23) \times 10^6$	
4d: median	$807(18) \times 10^1$	$379(11) \times 10^2$	$117(07) \times 10^3$	
4d: maximum	$13(11) \times 10^7$	$21(07) \times 10^8$	$22(21) \times 10^9$	

realizations were drawn using the pseudo-random-number generators RANMAR (Ref. 25) and RANLUX (Ref. 26) (luxury level 4). In the simulations themselves we always employed the RANMAR generator due to CPU time considerations.

For each realization  $\mathcal{J}$  the simulation consisted of three steps:

(i) Construction of the weight function (3). Here we employed an improved variant of the accumulative stochastic iteration scheme discussed in Ref. 27, algorithmic details will be published elsewhere.<sup>28</sup> The iteration was stopped after at least four tunneling events

$$(q=0) \rightarrow (q=\pm 1) \quad \text{and back} \quad (4)$$

occurred. Our precise request was in 3d 10 tunneling events for  $L=4, 6$ , and 8, and 20 events for  $L=12$ , but for a few cases with only four events requested. In 4d it was 10 for  $L=4$ , 20 for  $L=6$ , and 20 to 30 for  $L=8$ . In few cases, the system was tunneling so rarely between  $q=\pm 1$  that we decided to abort the run and restart with a different random number seed, which in most cases led (eventually after multiple tries) to improved tunneling performance. After the weight function is constructed and kept fixed, the average number of sweeps it takes to create a tunneling event (4) defines the autocorrelation time of the multioverlap algorithm which in the following is denoted by

$$\tau^{\text{muq}}. \quad (5)$$

Of course,  $\tau^{\text{muq}}$  depends on the realization  $\mathcal{J}$  at hand, and on the parameters used in phase (i): random number seed, number of tunneling events requested, etc.

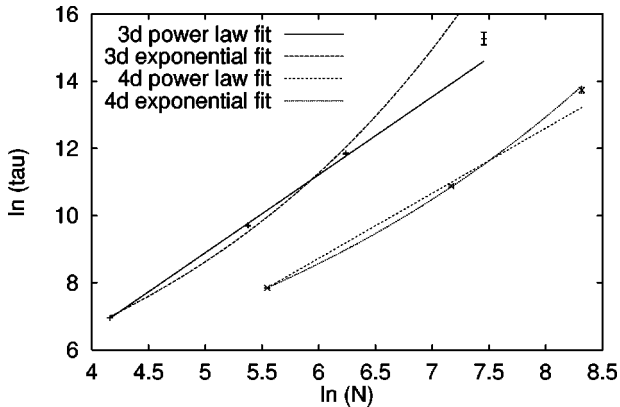


FIG. 2. Power-law and exponential fits for the mean multioverlap tunneling time  $[\tau^{\text{muq}}]_{\text{av}}$  in 3d and 4d.

(ii) Equilibration run. This run of  $n \times 65\,536$  sweeps was done to equilibrate the system for given fixed weight factors ( $n=1,4,16,32$  for 3d  $L=4,6,8,12$  and  $n=2,8,16$  for 4d  $L=4,6,8$ , respectively).

(iii) Production run. Each production run of data taking was concluded after at least 20 tunneling events as defined in Eq. (4) were recorded. To allow for standard reweighting in temperature we stored besides histograms of the Parisi overlap parameter also a time series of measurements for the order parameter, energies, and magnetizations of the two replica. The number of sweeps between two successive points in a time series is adjusted in such a way that each time series is made of 65 536 measurements. This is done by an adaptive data compression routine.<sup>28</sup> Together with the condition on the minimal number of tunneling events this ensures that the number of sweeps between two successive points in a time series is approximately proportional to  $\tau^{\text{muq}}$ . Some reweighting results were reported in Refs. 13 and 21, publication of others is intended.<sup>28</sup>

With each realization  $\mathcal{J}$  we associate the free-energy barrier  $F_B^q$  of the 1d Metropolis-Markov chain<sup>29</sup> which has the canonical  $P_{\mathcal{J}}(q)$  probability density as its equilibrium distribution. The transition probabilities  $T_{i,j}$  are given by

$$T = \begin{bmatrix} 1 - w_{2,1} & w_{1,2} & 0 & \dots \\ w_{2,1} & 1 - w_{1,2} - w_{3,2} & w_{2,3} & \dots \\ 0 & w_{3,2} & 1 - w_{2,3} - w_{4,3} & \dots \\ 0 & 0 & w_{4,3} & \dots \\ \vdots & \vdots & \vdots & \ddots \end{bmatrix}, \quad (6)$$

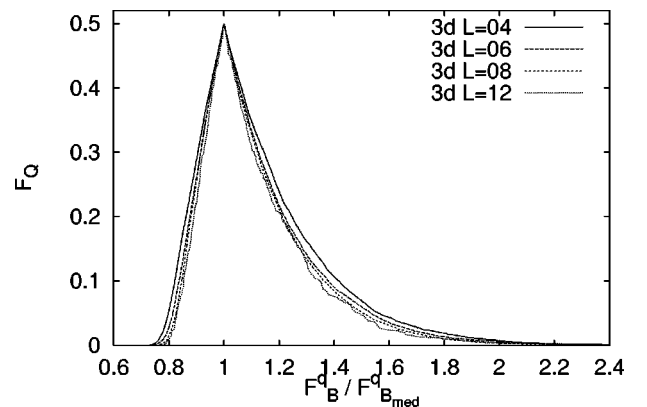


FIG. 3. Distribution function  $F_Q$  (13) for the 3d overlap barriers (9) in units of their median value.

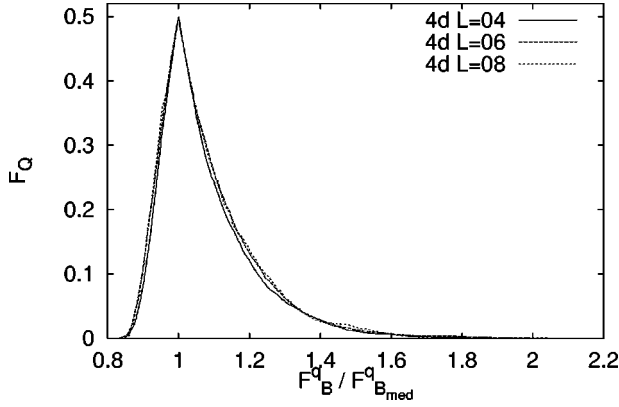


FIG. 4. Distribution function  $F_Q$  (13) for the  $4d$  overlap barriers (9) in units of their median value.

where  $w_{i,j}$  ( $i \neq j$ ) is the probability of the Metropolis-Markov chain to jump from state  $q=q_j$  to  $q=q_i$  ( $q_i = i/N, i \in [-N, -N+2, \dots, +N]$ ),

$$w_{i,j} = \frac{1}{2} \min \left( 1, \frac{P_{\mathcal{J}}(q_i)}{P_{\mathcal{J}}(q_j)} \right). \quad (7)$$

$T$  fulfills the detailed balance condition (with  $P_{\mathcal{J}}$ ) and as a consequence it has only real eigenvalues. The largest eigenvalue (equal to one) is nondegenerate, and the second largest eigenvalue  $\lambda_1$  determines the autocorrelation time of the chain,

$$\tau_B^q = \frac{1}{N(1-\lambda_1)}, \quad (8)$$

and we define the associated free-energy barrier for realization  $\mathcal{J}$  as

$$F_B^q = \ln(\tau_B^q). \quad (9)$$

For the simple double-peak situation of first-order phase transitions the autocorrelation time  $\tau_B^q$  is proportional to the ratio  $P_{\mathcal{J}}^{\max}/P_{\mathcal{J}}^{\min}$  where

$$P_{\mathcal{J}}^{\max} = P_{\mathcal{J}}(q_{\max}) = \max_q [P_{\mathcal{J}}(q)] \quad \text{and}$$

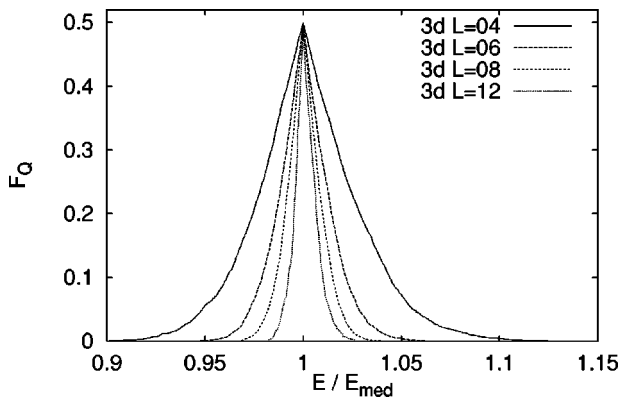


FIG. 5. Distribution function  $F_Q$  (13) for the  $3d$  energies (2) in units of their median value.

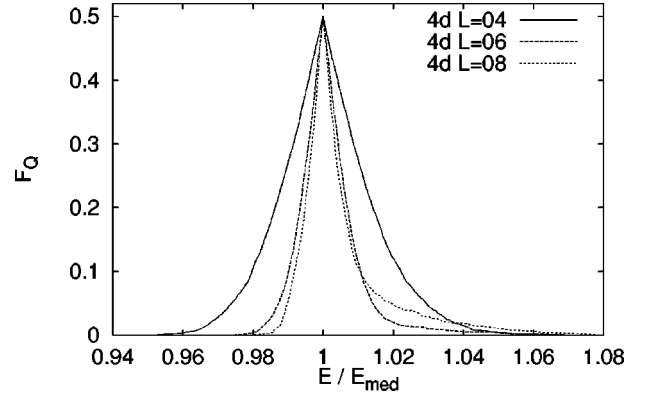


FIG. 6. Distribution function  $F_Q$  (13) for the  $4d$  energies (2) in units of their median value.

$$P_{\mathcal{J}}^{\min} = \min_{0 < q < |q_{\max}|} [P_{\mathcal{J}}(q)],$$

i.e.,  $F_B^q = \ln[P_{\mathcal{J}}^{\max}/P_{\mathcal{J}}^{\min}] + \text{const}$ . This leads in  $3d$  to  $\tau_B^q \sim e^{\sigma A_{\min}}$  and  $F_B^q \sim \sigma A_{\min} + \text{const}$ , where  $A_{\min}$  is the minimal area between the coexisting phase regions and  $\sigma$  is the interfacial tension. Equation (9) is the appropriate generalization to a situation involving multiple minima and maxima. The autocorrelation time  $\tau_B^q$  has to be regarded as a lower limit to the canonical autocorrelation time  $\tau^{\text{can}}$  for the Markov process where the spin variables are the dynamical degrees of freedom. The definition (8) takes only barriers in  $q$  into account but not other barriers which may well exist in the multidimensional configuration space.

The matrix  $T$  in Eq. (6) is tridiagonal and sign symmetric. This special form allows for easy calculation of all its eigenvalues.<sup>30</sup> The realizations with the largest thus obtained free-energy barriers in  $3d$  and  $4d$  are depicted in Fig. 1. Both do not show a complicated landscape, but a plain two-peak structure. Besides the canonical  $P_{\mathcal{J}}(q)$  probability densities the essentially flat probability densities  $P_{\mathcal{J}}^{\text{muq}}(q)$  of the multioverlap simulation are also indicated in the figure. Both  $P_{\mathcal{J}}(q)$  probability densities take their minimum at  $q=0$  and we have  $P_{\mathcal{J}}^{\max}/P_{\mathcal{J}}^{\min} > 10^8$  in  $3d$  ( $L=8$ ) and  $P_{\mathcal{J}}^{\max}/P_{\mathcal{J}}^{\min} > 10^6$  in  $4d$  ( $L=8$ ); compare also Table II. The improvement factors in computer time are directly proportional and close to these numbers which reflect the enhancements in visits of  $P_{\mathcal{J}}(0)$

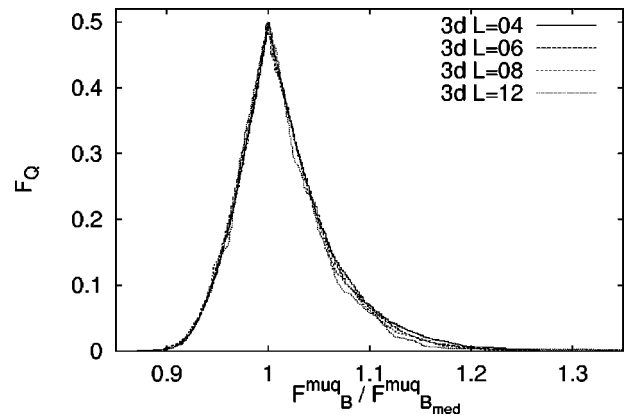


FIG. 7. Distribution function  $F_Q$  (13) for the  $3d$  barriers (14) of the multioverlap algorithm in units of their median value.

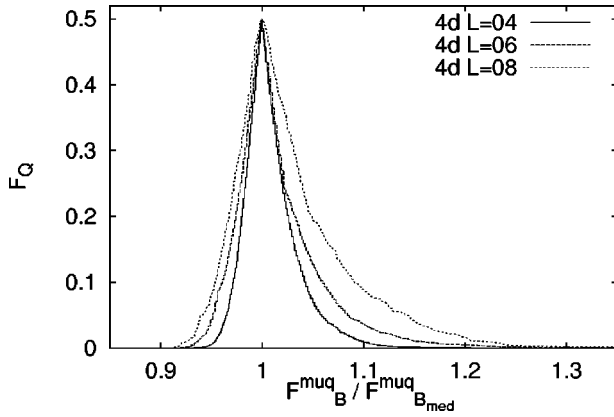


FIG. 8. Distribution function  $F_Q$  (13) for the  $4d$  barriers (14) of the multioverlap algorithm in units of their median value.

as compared to canonical simulations. Multiplying the improvement factors with the average CPU times needed by the multioverlap algorithm for a single realization on lattices of this size (see Table I), it becomes clear that exploration of such barriers by means of a canonical MC simulation is simply impossible.

We conclude this section with remarks about the performance of the algorithm and implications on the physics of the system. The multioverlap algorithm flattens the free-energy barriers  $F_B^q$ . If they were the only cause for the slowing down of the canonical dynamics, the multioverlap autocorrelation time should be dominated by a random-walk behavior between  $q = -1$  and  $q = +1$  and scale proportional to  $N$  (in units of sweeps). Fitting the estimates of the mean autocorrelation time  $[\tau^{\text{muq}}]_{\text{av}}$ , where the average is with respect to the realizations  $\mathcal{J}$ , to the power-law form  $\ln([\tau^{\text{muq}}]_{\text{av}}) = a + z \ln(N)$  gives  $z = 2.32 \pm 0.07$  in  $3d$  and  $z = 1.94 \pm 0.02$  in  $4d$ . The fits are depicted in Fig. 2. Their quality is bad, nevertheless they show that the slowing down is quite off from the theoretical optimum  $z = 1$ . Exponential fits  $\ln([\tau^{\text{muq}}]_{\text{av}}) = c_0 + c_1 N$  are also depicted in the figure. Whereas in  $3d$  the exponential fit is far worse than the power-law fit, it is the other way around in  $4d$ . Hence, the smaller  $z$  value in  $4d$  should not be taken seriously.

The physically important conclusion is: the observed large autocorrelation times demonstrate that, in the model

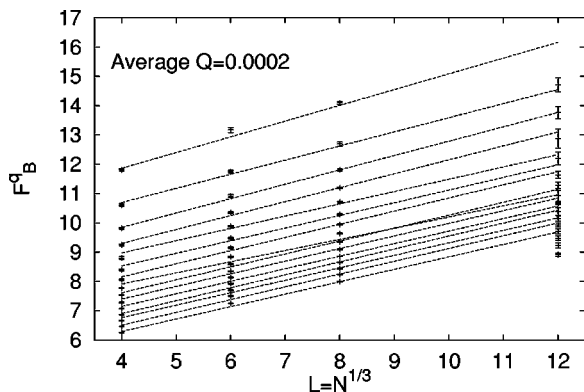


FIG. 9. Fits (15) of the  $3d$  free-energy barriers  $F_B^q$  versus  $N^{1/3}$  corresponding to the exponential finite-size scaling behavior (16) of  $\tau_B^q$ . From down to up, the lines are at  $16F = 1, 3, 5, 7, 9, 11, 12, 13, 14$ , and  $15$ .

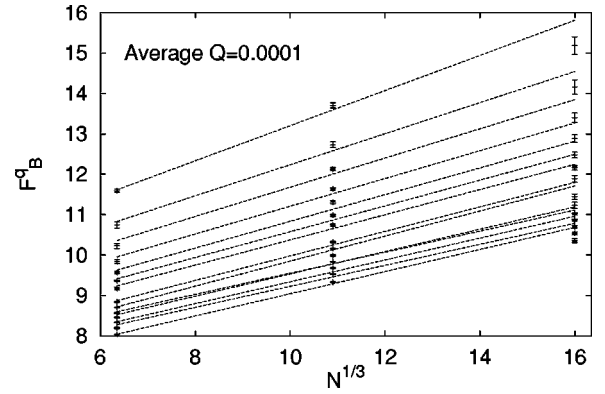


FIG. 10. Fits (15) of the  $4d$  free-energy barriers  $F_B^q$  versus  $N^{1/3}$  corresponding to the exponential finite-size scaling behavior (16) of  $\tau_B^q$ . From down to up, the lines are at  $16F = 1, 3, 5, 7, 9, 11, 12, 13, 14$ , and  $15$ .

considered, canonical overlap barriers are not an exclusive cause for the slowing down of spin-glass dynamics below the freezing temperature. Therefore  $\tau_B^q$  has to be a lower bound of the full canonical autocorrelation time  $\tau^{\text{can}}$ :

$$\tau_B^q < \tau^{\text{can}}. \quad (10)$$

One should understand  $q$  as one relevant direction in a complex, multidimensional configuration space. By depicting free-energy barriers as function of  $q$  one projects on this direction and averages results over all other directions.

### III. BARRIER RESULTS

We analyze our free-energy barrier densities relying on a variant of the cumulative distribution function  $F$ . For a set of sorted data

$$x_1 < x_2 < \dots < x_n \quad (11)$$

the (empirical) cumulative distribution function  $F(x)$ , see, for instance, Ref. 31 is defined by

$$\frac{i}{n} - \frac{1}{2n} \leq F(x) \leq \frac{i}{n} + \frac{1}{2n} \quad \text{for } x_i \leq x \leq x_{i+1}, \quad (12)$$

where we use a straight-line interpolation in between. Next we define a peaked distribution function<sup>32</sup> as introduced in Ref. 33:

$$F_Q(x) = \begin{cases} F(x) & \text{for } F(x) \leq 0.5; \\ 1 - F(x) & \text{for } F(x) \geq 0.5. \end{cases} \quad (13)$$

This function peaks at the median  $x_{\text{med}}$  of the data and takes there the value  $F_Q = 0.5$ . For self-averaging data  $x$  the function  $F_Q$  collapses in the infinite volume to

$$F_Q(x) = \begin{cases} 0.5 & \text{for } x = \bar{x}; \\ 0 & \text{otherwise.} \end{cases}$$

Here  $\bar{x}$  is the mean value. For non-self-averaging quantities the width of  $F_Q$  stays finite. The concept carries over to observables which diverge in the infinite volume limit, when

TABLE III. Fit parameters for the free-energy barriers fits (15);  $Q < 0.003$  for all cases.

$F$	$3d$		$4d$	
	$a_1$	$a_2$	$a_1$	$a_2$
1/16	4.59(2)	0.424(03)	6.30(02)	0.274(03)
4/16	5.13(3)	0.442(04)	6.77(03)	0.276(03)
8/16	6.38(4)	0.382(05)	7.13(05)	0.301(06)
12/16	7.39(6)	0.476(11)	7.77(11)	0.344(10)
15/16	9.71(9)	0.538(14)	8.85(12)	0.435(15)

on each lattice size results are expressed in units of the respective median value, i.e., instead of an observable  $X$  the ratio  $x = X/X_{\text{med}}$  is used.

### A. Lack of self-averaging

For the free-energy barriers (9) we have depicted our thus obtained  $F_Q(F_B^q/F_{B,\text{med}}^q)$  functions in Figs. 3 ( $3d$ ) and 4 ( $4d$ ). For each lattice the measured  $F_B^q$  values were first sorted as function of  $\mathcal{J}$  such that

$$F_{B,1}^q < F_{B,2}^q < \dots < F_{B,n}^q,$$

where  $n$  is the number of realizations  $\#\mathcal{J}$  given in Table I. Subsequently,  $F_{B,\text{med}}^q$  was calculated as

$$F_{B,\text{med}}^q = \frac{1}{2}(F_{B,n/2}^q + F_{B,1+n/2}^q) \quad (n \text{ is even in our cases}),$$

and  $F_Q$  computed for  $x = F_B^q/F_{B,\text{med}}^q$ .

Both figures support that  $F_B^q$  is a non-self-averaging quantity. This is stronger in  $4d$  than in  $3d$ , because the inner lines belong in  $3d$  to the larger lattices, whereas in  $4d$  it is the other way around. However, in both cases there are marginal finite-size effects, whereas finite-size dependence of self-averaging is expected to be rather strong. This becomes obvious when comparing with an observable which is supposed to be self-averaging. Namely, Figs. 5 ( $3d$ ) and 6 ( $4d$ ) depict the same analysis for the internal energy (2). In  $3d$  self-averaging of this quantity is obvious, whereas in  $4d$  there is an irregularity when going from  $L=6$  to  $L=8$ . As our simulation temperature in  $4d$  is quite low, we think that this be-

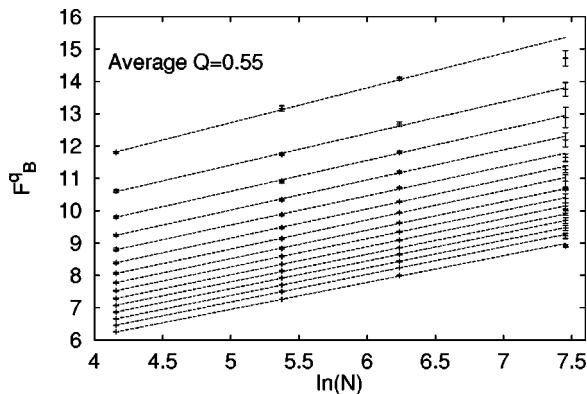


FIG. 11. Fits (18) of the  $3d$  free-energy barriers  $F_B^q$  versus  $\ln(N)$  corresponding to the power-law finite-size scaling behavior (17) of  $\tau_B^q$ . From down to up, the lines are at  $16 F = 1, 3, 5, 7, 9, 11, 12, 13, 14$ , and  $15$ .

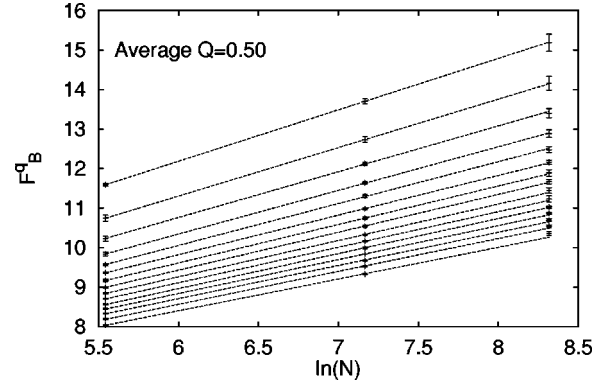


FIG. 12. Fits (18) of the  $4d$  free-energy barriers  $F_B^q$  versus  $\ln(N)$  corresponding to the power-law finite-size scaling behavior (17) of  $\tau_B^q$ . From down to up, the lines are at  $16 F = 1, 3, 5, 7, 9, 11, 12, 13, 14$ , and  $15$ .

havior is related to ground-state irregularities on small lattices (only the corresponding half of the distribution is affected). For both  $3d$  and  $4d$  the peaked distribution function of the energy is strongly concentrated around  $E/E_{\text{med}} = 1$ , whereas the overlap barrier distributions are much broader.

It is generally believed that, in contrast to the equilibrium autocorrelation times considered here, nonequilibrium autocorrelations are self-averaging.<sup>10</sup> No sample-to-sample deviations have been reported for real experiments<sup>6</sup> and self-averaging is also used for measurements of nonequilibrium properties in MC simulations.<sup>11,12</sup>

The multioverlap algorithm eliminates the free-energy barriers which are visible in the  $P_{\mathcal{J}}(q)$  probability densities. Let us therefore focus on the autocorrelation times of this algorithm and its barriers defined by

$$F_B^{\text{muq}} = \ln(\tau_B^{\text{muq}}). \quad (14)$$

We perform the analysis along our previous lines and show in Figs. 7 ( $3d$ ) and 8 ( $4d$ ) the thus obtained  $F_Q(F_B^{\text{muq}}/F_{B,\text{med}}^{\text{muq}})$  functions. Lack of self-averaging is even more obvious than for  $F_B^q$ . In Fig. 7 ( $3d$ ) there are (within the statistical accuracy) no finite-size effects visible and Fig. 8 ( $4d$ ) exhibits a strong anti-self-averaging trend: Results for the larger lattices move to the outside instead of to the inside.

### B. Finite-size scaling behavior

In this final part of Sec. III we discuss how data (experimental or MC) for non-self-averaging observables may be analyzed such that comparisons of results from different groups become possible. One has to investigate many samples and should report the finite-size scaling behavior for fixed values of the cumulative distribution function  $F$  (12). In particular this includes  $F = 1/2$  which defines the median value. We exemplify this for the overlap autocorrelation time  $\tau_B^q$  (8), but the method applies for non-self-averaging observables in general.

From Figs. 3 and 4 it is obvious that the autocorrelation times  $\tau_B^q$  will have long tails towards large values. This implies that the mean value over all samples is a rather erratic quantity which is dominated by a few rare realizations. Table II collects the mean, median ( $F = 1/2$ ), and maximum [ $F$

TABLE IV. Free-energy barriers fits (18): Fit parameters and goodness of fit.

$F$	$3d$			$4d$		
	$\ln(c)$	$\alpha$	$Q$	$\ln(c)$	$\alpha$	$Q$
1/16	2.80(03)	0.830(06)	0.04	3.58(05)	0.804(08)	0.05
4/16	3.30(04)	0.857(08)	0.77	3.68(06)	0.860(08)	0.13
8/16	4.10(06)	0.883(10)	0.52	3.68(11)	0.958(18)	0.71
12/16	5.37(11)	0.930(20)	0.51	3.71(22)	1.105(32)	0.81
15/16	7.35(14)	1.075(28)	0.02	4.37(26)	1.302(42)	0.94

$=1-1/(2n)]$  values for  $\tau_B^q$ . The numbers in parentheses indicate error bars in the last digits of the quantity given before. The results show that contributions of the maximum values dominate to a large extent the mean values (just divide the maximum values by the number of realizations and compare the results with the mean values). The maximum values rely on realizations  $\mathcal{J}$  of likelihood  $1/n$ , what explains their very large errors. In contrast to the mean and the maximum, results for fixed  $F$  remain well defined as long as  $F$  stays away from its extreme values  $1/n$  and  $1-1/n$ . In particular, note that samples with relaxation times too long to be measured can still contribute to determine the correct  $F$  values for smaller relaxation times.

In the following we focus on our results for the free-energy barriers  $F_B^q$  at  $F=i/16$  with  $i=1, \dots, 15$ . For each  $F$  value we performed fits to the form

$$F_B^q = a_1 + a_2 N^{1/3} \quad (15)$$

which corresponds to the exponential finite-size scaling behavior

$$\tau_B^q = e^{a_1} e^{a_2 N^{1/3}} \quad (16)$$

suggested by investigations of autocorrelation times and barriers in the mean-field limit.<sup>16–20</sup> These fits are depicted in Figs. 9 and 10. Examples of the fit parameters  $a_1$  and  $a_2$  are collected in Table III; for all fits given there, the goodness-of-fit parameter  $Q$  (Ref. 31) is smaller than 0.003. The average  $Q$  over all 15 fits is given in the figures. For consistent fits the expectation for the  $Q$  average is  $1/2$  and the quality of our  $3d$  and  $4d$  exponential fits is unacceptable. We therefore try a power-law fit

$$\tau_B^q = c N^\alpha, \quad (17)$$

which corresponds to a fit of the form

$$F_B^q = \ln(c) + \alpha \ln(N). \quad (18)$$

These fits are depicted in Figs. 11 and 12. In  $3d$  as well as in  $4d$  the average  $Q$  value is now almost perfect. Examples of the power-law fit parameters and  $Q$  values are given in Table IV. They indicate that the distribution of  $Q$  values is less perfect than their mean. Such uncertainties are an intrinsic limitation of MC simulations and become particularly severe when one is, as in our investigation, limited to rather small-

sized systems. Having these limitations in mind, the overall quality of the power-law fits is remarkably good. Our data favor them strongly over the exponential behavior.

As function of  $F$  the exponent  $\alpha = \alpha(F)$  varies smoothly and covers in  $4d$  a range from 0.8 at  $F=1/15$  to 1.3 at  $F=15/16$ . In  $3d$  the range is somewhat smaller, see Table IV. Fits for  $F > 15/16$  become erratic and it makes little sense to report them. A similar analysis for the autocorrelation times of the multioverlap algorithm gives exponents  $\alpha(F)$  which are larger,

$$\alpha^{\text{muq}}(F) \approx \alpha_B^q(F) + 1.$$

This reiterates and sharpens our previous observation that relevant barriers exist, which are invisible in the overlap variable  $q$ .

#### IV. SUMMARY AND CONCLUSIONS

We have investigated free-energy barriers in the Parisi order parameter (1). The results are sample dependent and non-self-averaging on the (admittedly rather small) simulated systems. The power-law behavior (17) of the Markov autocorrelation times  $\tau_B^q$  as defined in Eq. (8) is favored over the exponential behavior (16). To the extent that this behavior extrapolates to the infinite volume limit and that our methods relate to those of Refs. 16–20, it means that both  $3d$  and  $4d$  are quite far away from the  $d \rightarrow \infty$  mean-field theory limit. As relevant barriers are still found in the autocorrelations of the multioverlap algorithm, such a relation is far from clear.

#### ACKNOWLEDGMENTS

B.B. would like to thank Wolfgang Grill for his hospitality during an extended stay at Leipzig University in the framework of the *International Physics Studies Program*. Most numerical simulations were performed on the T3E computer of CEA in Grenoble under Grant No. p526. Additional calculations were done on T3E computers of ZIB in Berlin under Grant No. bvp101, and of NIC in Jülich under Grant No. hzm091, and on Alpha workstations at FSU. This research was partially funded by the Department of Energy under Contract Nos. DE-FG02-97ER41022 and DE-FG05-85ER2500. We thank all institutions for their generous support.

\*Electronic address: berg@scri.fsu.edu

†Electronic address: billoir@spht.saclay.cea.fr

‡Electronic address: wolffhard.janke@itp.uni-leipzig.de

<sup>1</sup>*Spin Glasses and Random Fields*, edited by A. P. Young (World Scientific, Singapore, 1997).

<sup>2</sup>K.H. Fischer and J.A. Hertz, *Spin Glasses* (Cambridge University

- Press, Cambridge, England, 1991).
- <sup>3</sup>M. Mézard, G. Parisi, and M.A. Virasoro, *Spin Glass Theory and Beyond* (World Scientific, Singapore, 1987).
- <sup>4</sup>K. Binder and A.P. Young, *Rev. Mod. Phys.* **58**, 801 (1986).
- <sup>5</sup>C.A.M. Mulder, A.J. van Duyneveldt, and J.A. Mydosh, *Phys. Rev. B* **23**, 1384 (1981); **25**, 515 (1982).
- <sup>6</sup>P. Granberg, P. Svedlindh, P. Nordblad, L. Lundgren, and H.S. Chen, *Phys. Rev. B* **35**, 2075 (1987); E. Vincent, J. Hammann, M. Ocio, J.-P. Bouchaud, and L.F. Cugliandolo, in *Complex Behaviour of Glassy Systems*, edited by M. Rubi, Lecture Notes in Physics Vol. 492 (Springer-Verlag, Berlin, 1997), pp. 184-219, and references given therein.
- <sup>7</sup>G. Parisi, *Phys. Rev. Lett.* **43**, 1754 (1979).
- <sup>8</sup>D.S Fisher and D.A. Huse, *Phys. Rev. B* **38**, 386 (1988).
- <sup>9</sup>L.F. Cugliandolo and J. Kurchan, *Phys. Rev. Lett.* **71**, 173 (1993); *J. Phys. A* **27**, 5749 (1994).
- <sup>10</sup>J.-P. Bouchaud, L.F. Cugliandolo, J. Kurchan, and M. Mézard, in *Spin Glasses and Random Fields* (Ref. 1), p. 161 ff., Sec. 3.1.
- <sup>11</sup>S. Franz and H. Rieger, *J. Stat. Phys.* **79**, 749 (1995).
- <sup>12</sup>E. Marinari, G. Parisi, F. Ricci-Tersenghi, and J.J. Ruiz-Lorenzo, *J. Phys. A* **31**, 2611 (1998).
- <sup>13</sup>B.A. Berg and W. Janke, *Phys. Rev. Lett.* **80**, 4771 (1998).
- <sup>14</sup>G.M. Torrie and J.P. Valleau, *J. Comput. Phys.* **23**, 187 (1977); B.A. Berg and T. Neuhaus, *Phys. Rev. Lett.* **68**, 9 (1992); B.A. Berg and T. Celik, *ibid.* **69**, 2292 (1992); W. Janke and S. Kappler, *ibid.* **74**, 212 (1995); B. Hesselbo and R. Stinchcombe, *ibid.* **74**, 2151 (1995).
- <sup>15</sup>B.A. Berg, U. Hansmann, and T. Neuhaus, *Phys. Rev. B* **47**, 497 (1993); *Z. Phys. B: Condens. Matter* **90**, 229 (1993).
- <sup>16</sup>N.D. Mackenzie and A.P. Young, *Phys. Rev. Lett.* **42**, 301 (1982); *J. Phys. C* **16**, 5321 (1983).
- <sup>17</sup>K. Nemoto, *J. Phys. A* **21**, L287 (1988).
- <sup>18</sup>G.J. Rodgers and M.A. Moore, *J. Phys. A* **22**, 1085 (1989).
- <sup>19</sup>D. Vertechi and M.A. Virasoro, *J. Phys. (France)* **50**, 2325 (1989).
- <sup>20</sup>R.N. Bhatt, S.G.W. Colborne, M.A. Moore, and A.P. Young (unpublished), see Ref. 18.
- <sup>21</sup>W. Janke, B.A. Berg, and A. Billoire, *Ann. Phys. (Leipzig)* **7**, 544 (1998).
- <sup>22</sup>S.F. Edwards and P.W. Anderson, *J. Phys. F: Met. Phys.* **5**, 965 (1975).
- <sup>23</sup>N. Kawashima and A.P. Young, *Phys. Rev. B* **53**, R484 (1996).
- <sup>24</sup>D. Badoni, J.C. Ciria, G. Parisi, F. Ritort, J. Pech, and J.J. Ruiz-Lorenzo, *Europhys. Lett.* **21**, 495 (1993).
- <sup>25</sup>G. Marsaglia, A. Zaman, and W.W. Tsang, *Stat. Prob. Lett.* **8**, 35 (1990).
- <sup>26</sup>M.L. Lüscher, *Comput. Phys. Commun.* **79**, 100 (1994).
- <sup>27</sup>B.A. Berg, *J. Stat. Phys.* **82**, 323 (1996).
- <sup>28</sup>B.A. Berg, A. Billoire, and W. Janke (unpublished).
- <sup>29</sup>N. Metropolis, A.W. Rosenbluth, M.N. Rosenbluth, A.H. Teller, and E. Teller, *J. Chem. Phys.* **21**, 1087 (1953).
- <sup>30</sup>We used the EISPACK subroutines `figi` and `imtqll` which are available on the web at Bell Labs: <http://netlib.bell-labs.com/netlib/eispack/index.html>
- <sup>31</sup>W.H. Press, B.P. Flannery, S.A. Teukolsky, and W.T. Vetterling, *Numerical Recipes* (Cambridge University Press, Cambridge England, 1986).
- <sup>32</sup> $Q$  refers to statistical  $Q$  tiles and  $q$  to the Parisi overlap parameter.
- <sup>33</sup>B.A. Berg (unpublished).